

UPDATED AND EXPANDED OPAL EQUATION-OF-STATE TABLES: IMPLICATIONS FOR HELIOSEISMOLOGY

F. J. ROGERS¹ AND A. NAYFONOV^{1,2}

Received 2002 April 15; accepted 2002 May 20

ABSTRACT

We are in the process of updating and extending the OPAL equation-of-state (EOS) and opacity data to include low-mass stars. The EOS part of that effort now is complete, and the results are described herein. The new data cover main-sequence stars having mass $\geq 0.1 M_{\odot}$. As a result of the more extreme matter conditions encountered with low-mass stars, we have added new physics. The electrons are now treated as relativistic, and we have improved our treatment of molecules. We also consider the implications of the new results for helioseismology.

Subject headings: atomic processes — equation of state — Sun: oscillations

1. INTRODUCTION

The OPAL equation-of-state (EOS; Rogers, Swenson, & Iglesias 1996, hereafter RSI96) and opacity tables (Iglesias & Rogers 1996) have frequently been used to model stars. The temperature-density range of the RSI96 tables is sufficient to study main-sequence stars having masses greater than about $0.8 M_{\odot}$. The thermodynamic properties of these stars are those of a weakly coupled partially ionized plasma. Nonideal corrections to the pressure never exceed about 10% for $M \geq 0.8 M_{\odot}$. Nevertheless, simple models that invoke heuristic arguments to cut off the divergence of the atomic partition function and to approximate the size of the nonideal plasma contribution can vary by several percent in pressure and energy and substantially more in the thermodynamic derivatives of the EOS. Discrepancies of this size are far too large to analyze helioseismic data, which are capable of estimating the sound speed to a few parts in 10^4 (Christensen-Dalsgaard et al. 1996). Similar EOS data are also needed to model less massive stars, which are composed of substantially more nonideal plasmas. Consequently, we have undertaken an effort to extend the existing OPAL database to include stars having $M \geq 0.1 M_{\odot}$. Herein we describe the EOS part of that effort.

In the Saha approach and its modifications the divergence of the atomic partition function is removed by introducing ad hoc criteria for screening bound states into the continuum, resulting in unphysical discontinuities in the EOS. This is a consequence of the fact that the Coulomb correlation effects on the continuum states are ignored, except for a partial contribution that enters through the Debye-Hückel correction when it is included in the free energy. In recent implementations of this approach these discontinuities in the EOS are eliminated by introducing an occupation probability (reduced statistical weight), w , that a composite particle (i.e., ion, atom, molecule) finds itself in an environment where the bound electrons are highly localized around a single nucleus. The quantity $1 - w$ is then the probability that, as a result of interactions with nearby neighbors, the

bound electrons are in delocalized quasi-continuum states (Däppen, Anderson, & Mihalas 1987; Hummer & Mihalas 1988; Mihalas, Däppen, & Hummer 1988; hereafter MDH88). This is an intuitive approach whose success depends on how well w is determined. Nevertheless, there is no a priori theory for determining w or the quasi-continuum state contribution. In contrast, the OPAL EOS and opacity calculations are based on an activity expansion of the grand canonical partition function. The starting point in this approach is the Coulomb interactions between all the fundamental constituents, i.e., electrons and nuclei, in the system. The effect of multiparticle Coulomb interactions on bound states arises naturally, without the introduction of ad hoc assertions. Consequently, the thermodynamic properties are continuous functions of temperature and density. This method has been developed over a number of years and is described elsewhere (Rogers 1981, 1986, 1994, 2001b).

As the stellar mass decreases toward the cutoff at the bottom of the main sequence, the nonideal corrections to the EOS increase substantially. Pressure ionization becomes important for $M < 0.3 M_{\odot}$. The inclusion of an increasing number of terms in the activity expansion, after elimination of the activity, results in a systematic expansion in the density. The order of expansion (Rogers 1981) used to calculate the updated EOS tables should be accurate for stellar tracks having $M \geq 0.3 M_{\odot}$ but starts to degrade for less massive stars. It is difficult to give an estimate of the size of the errors in the tabulated results. The Coulomb coupling parameter,

$$\Gamma = \frac{\langle Z^2 \rangle}{kTa} e^2, \quad (1)$$

where $\langle Z^2 \rangle$ is the average square charge and a is the ionosphere radius, never exceeds 1.5 along the $M = 0.3 M_{\odot}$ track but approaches 4.5 at some locations along the $M = 0.1 M_{\odot}$ track. The maximum error in the OPAL nonideal pressure calculations should be less than 5% at the most nonideal parts of the $M = 0.3 M_{\odot}$ track (Rogers & Dewitt 1973; Rogers 1981). This translates into errors of 1%–2% in the total pressure. The size of the errors increases somewhat for the $M = 0.1 M_{\odot}$ track but diminishes rapidly with increasing mass for $M > 0.3 M_{\odot}$.

The EOS calculations reported herein include relativistic electrons, new methods for treating neutral-neutral and

¹ Lawrence Livermore National Laboratory, P.O. Box 808, Livermore, CA 94550.

² Current address: Teradyne Incorporated, 30801 Agoura Road, Agoura Hills, CA 91301.

neutral-plasma interactions, and an improved, but still incomplete, treatment of molecules. These improvements will be discussed in § 2. A discussion of the results and comparisons with other work will be given in § 3. The improved calculations have some implications for helioseismology that will be discussed in § 4.

2. NEW AND IMPROVED PHYSICS

2.1. Relativistic Electrons

The RSI96 tables cover a temperature-density range where relativistic effects are small and so were not included. This reasoning failed to consider the high accuracy of helioseismic data. Elliot & Kosovichev (1998, hereafter EK98) showed that this missing physics is easily detected by helioseismic inversions of the solar oscillations. The largest effect of relativity occurs in the ideal electron contribution to the EOS. The relativistic Fermi integral is given by

$$F_k(\alpha, T_r) = \frac{1}{\Gamma(k+1)} \int_0^\infty \frac{x \sqrt{1 + (T_r x/2)^2}}{e^{x-\alpha} + 1} dx, \quad (2)$$

where $\Gamma(k+1)$ is the gamma function, $\alpha = \mu/kT$, μ is the chemical potential, and $T_r = kT/m_e c^2$. Approximate expressions for the relativistic Fermi integral exist in various limits (Cox & Guili 1968). A number of quadrature methods have been used for numerical calculation of $F_k(\alpha, T_r)$ (Sugar 1991; Aparico 1998; Gong et al. 2001c). In this work we have used a four-point Gaussian quadrature method, due to D. Harwood (1968, unpublished), that breaks the integration range into 2^n partitions. The parameter n is sequentially increased until the desired level of accuracy is obtained by comparison with the result for 2^{n-1} partitions. The ideal relativistic electron pressure is given by

$$P_e^{\text{id}} = \frac{2kT}{\lambda_e^3} \left(F_{3/2} + \frac{5}{4} T_r F_{5/2} \right), \quad (3)$$

where

$$\lambda_e = \left(\frac{2\pi\hbar^2}{m_e kT} \right)^{1.2} \quad (4)$$

is the electron thermal de Broglie wavelength. Equation (3) replaces the degenerate nonrelativistic limit of this expression in equation (61) of Rogers (1981). The corresponding effect on other thermodynamic properties is obtained from a numerical solution of a multicomponent generalization of equations (15) and (61) of that same paper. The electron exchange integral is also modified in the relativistic regime. We have used the expansion of Stolzmann & Blöcker (1996) to calculate the relativistic correction to electron exchange. We are not aware of relativistic generalizations of higher order terms in the activity expansion. For these terms we have simply replaced the nonrelativistic Fermi function by $F_k(\alpha, T_r)$.

2.2. Improved Activity Expansion

The activity expansion works well for partially ionized systems because the activity for species i ,

$$z_i = (2s_i + 1) \lambda_i^{-3} e^{u_i/kT}, \quad (5)$$

where s_i is the particle spin and λ_i is the thermal de Broglie wavelength for particles of mass m_i , involves the chemical potential and is thus the natural expansion to use for reacting systems. In contrast, the virial expansion has poor convergence properties when material is partially ionized (Rogers & Dewitt 1973). At very low temperature, where only atoms and molecules exist, the opposite is true. In the intermediate range where neutral particles and ions exist simultaneously, neither expansion works very well. In the present work we use a method that combines the best features of both expansions and is able to handle all three regions with equal level of approximation (Rogers 2001a).

2.3. Factorization of Cluster Coefficients and Effective Potentials

The activity expansion used herein is developed in terms of the fundamental particle activities (eq. [5]). The lowest order term that will involve, for example, H_2 molecules, thus comes from b_{epp} , the fourth cluster coefficient for two electrons and two protons. The calculation of b_{epp} is in principle a four-body problem. In addition, because of the long range of the Coulomb interaction, b_{epp} is divergent. The diagrammatic resummation techniques used in the many-body activity expansion (Rogers 1981, 1994) replace the Coulomb interaction with the screened Coulomb interaction, so that the cluster coefficients are well behaved. When the temperature is low enough that both bound electrons are in $1s$ states, b_{epp} can be factored into a product of second cluster coefficients (Rogers & Dewitt 1973; Schlages & Kremp 1982) in the form $(b_{ep}^g)^2 b_{\text{HH}}$, where b_{ep}^g is the ground-state contribution to the second cluster coefficient resulting from electron-proton interactions and b_{HH} is the second cluster coefficient for $\text{H}(1s)\text{-H}(1s)$ interactions. As a result of their large mass compared to electrons, the H-H interactions can be calculated in the adiabatic approximation, giving rise to singlet and triplet potential energy curves (interaction potentials). In general, the cluster coefficients for other molecular interactions can also be factored into products of second cluster coefficients. Ab initio calculations exist for most of the atomic and molecular potential energy curves needed to calculate the EOS of a hydrogen-helium mixture that is both partially ionized and partially dissociated. In addition to atoms and their ions we have included H^- , H_2^+ , H_2 , He_2^+ , and HeH^+ in the updated EOS calculations. Figure 1 displays a number of the potential energy curves used in the present work to account for the interactions between these species. Additional potential energy curves (not displayed) used in these calculations were $p\text{-H}$ (Teller 1930), $p\text{-He}^+$ (Kolos & Peek 1976), He-H_2^+ (Hopper 1980), and He-H_2 (Shafer & Gordon 1973). We consider static atom-atom interactions between C, N, O, and Ne but do not consider any molecular interactions. The electron-atom potentials needed for these calculations were obtained from parametric potentials fitted to electron affinities or extrapolated from isoelectronic sequence data as described in Rogers (1988).

It is well known that the second cluster coefficient between particles i and j can be obtained from the Beth-

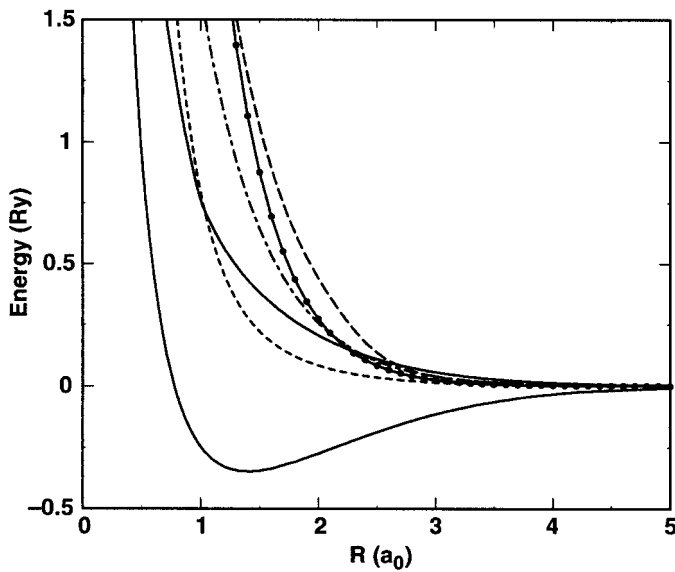


FIG. 1.—Potential energy curves. H singlet (lower solid line; Kolos & Wolniewicz 1965); H triplet (upper solid line); H-H₂ (short-dashed line; Partridge et al. 1993); H₂-H₂ (long-dashed line; Diep & Johnson 2000); He-He (solid line with circles; Cvetko et al. 1994); H-He (dot-dashed line; Tang & Yang 1990; Cvetko et al. 1994).

Uhlenbeck (1937) expression,

$$b_{ij} = 2^{1/2} \lambda_{ij}^3 \left[\sum_{nl} (2l+1) e^{-E_{nl}/kT} + \sum_l (2l+1) \int_0^\infty dq \frac{d\delta_l(q)}{dq} e^{q^2/2\mu_{ij}kT} \right], \quad (6)$$

where

$$\lambda_{ij} = (\hbar^2/2\mu_{ij}kT)^{1/2} \quad (7)$$

is the thermal de Broglie wavelength in center-of-mass coordinates, the E_{nl} are bound states, the $\delta_l(q)$ are scattering phase shifts for relative momentum q , and μ_{ij} is the reduced mass. It should be possible to generalize equation (6) to molecular interactions. However, as a result of the extra degrees of freedom associated with the vibrational-rotational states, the molecular case is more complex and has apparently never been worked out. We present arguments below that give some insight into the form of the molecular second cluster coefficient and are intended to motivate our calculations for molecules.

The total cluster coefficient for the H(1s)-H(1s) electronic configuration can be written in the form

$$b_{HH} = \frac{s_e}{2s_e + 1} b_{HH}^S + \frac{s_e + 1}{2s_e + 1} b_{HH}^T, \quad (8)$$

where b_{HH}^S is the singlet contribution, b_{HH}^T is the triplet contribution, and s_e is the electron spin. The singlet potential has a deep attractive well (see Fig. 1) giving rise to numerous vibrational-rotational states, while the triplet potential has only a very shallow attractive well. The bound-state part of b_{HH}^S involves sums over the vibrational-rotational quantum numbers ν and K . The form that the scattering-state contribution takes is not so obvious. At low temperature, to second order in the activity of hydrogen atoms, z_H , the

pressure is given by

$$\frac{P}{kT} = z_H + z_H^2 b_{HH}. \quad (9)$$

Since our starting point was a system of electrons and nuclei, equation (9) is obviously the result of some theoretical development. We will give a summary below that describes the procedure. Rogers (1974) showed that, in order to obtain a systematic expansion in the density, it is necessary to separate $z_H^2 b_{HH}$ into its bound-state (bs) and scattering-state (s) parts according to

$$z_H^2 b_{HH} = z_H^2 b_{HH}^{bs} + z_H^2 b_{HH}^s. \quad (10)$$

At low temperature the first term on the right-hand side (bs) acts linear in the activity of H₂ molecules, while the second acts quadratic in the activity for H atoms. In general, the cluster coefficient for N atoms is separated into N parts following a similar pattern. These terms are then reorganized based on their effective power in the activity. This gives an expression that selects the most important terms needed to account for the species that exist at a given temperature and density.

2.4. Divergences in Molecular Partition Functions

The H₂ molecule has an infinite number of electronic states of the type H(1s)-H(n, l) whose potential energy curves converge in the limit of large n to the H₂⁺(²Σ_g) potential curve (Sharp 1971). Consequently, the summation over internal electronic states diverges similar to H atoms. For high n the interacting electron is well outside the core of H₂⁺, so that for an isolated system it is effectively bound to a unitary point charge. The bound and scattering states of the interacting electron are therefore hydrogenic. Furthermore, the vibrational-rotational spectra of these highly excited electronic states are virtually identical to those of H₂⁺ and can be factored out. The contribution from the high- n electronic states to the partition function can therefore be obtained from a summation similar to the bracketed part of equation (6), both parts of which diverge in the isolated particle case. In the plasma, however, as a result of the exponential screening of Coulomb interactions, these terms are finite.

The states of the interacting electron relative to the H₂⁺ ground state can (in concept) be calculated from a parameterized spherically symmetric two-body potential that has a short-range attractive term due to interactions with the core and a long-range Coulomb tail. In the simple case in which the screening length is large compared to the ionic core size, the Coulomb tail of the parametric potential becomes exponentially screened, while the core term is unaffected. To get a crude approximation to the molecular component of b_{epp} , identified in the following by a prime, we assume that the vibrational-rotational states are uncoupled from the interacting electron, i.e., are the same as in H₂⁺, for all electronic states. This allows the cluster coefficient to be factored as follows:

$$b'_{epp} = 2\lambda_{ep}^6 \lambda_{HH}^3 e^{-E_{H_2^+}/kT} Q(T) \left[\sum_{nl} (2l+1) e^{-E_{nl}/kT} + \sum_l (2l+1) \int_0^\infty dq \frac{d\delta_l(q)}{dq} e^{q^2/2\mu_{eH_2^+}kT} \right], \quad (11)$$

where the λ_{ij} are given by equation (7), $E_{H_2^+}$ is the binding energy of H_2^+ relative to an isolated electron and two protons, and $Q(T)$ is the vibrational-rotational partition function of H_2^+ . The bound-state energies, E_{nl} , and phase shifts, $\delta_l(q)$, can be calculated from the parametric potential. Equation (11) should give the correct high- T result for b'_{epp} . As $n \rightarrow 1$, the vibrational-rotational spectrum will change appreciably and the scattering states will also be modified. As a result, the simple two-body potential picture is no longer realistic. It may be possible to use perturbation theory to account for these modifications. The main corrections will likely come from the vibrational-rotational states. Since these have already been accurately calculated (Waech & Bernstein 1967) and measured (Drabowski 1984), these corrections can easily be made.

2.5. Similarities in Atomic and Molecular Partition Functions

The reactions $e + p \leftrightarrow H$ and $e + H_2^+ \leftrightarrow H_2$ are similar in that two ions of opposite charge combine to form a neutral. In the case of H, after some expansion and reorganization of terms in the activity series (Rogers 1981, 1994), the summation over the ring diagrams and more complex ringlike diagrams gives a contribution $\propto (Z - 1)^2 z_H$ in the Debye-Hückel Coulomb interaction term (see eq. [44] of Rogers 1974). Thus, the net ring-sum contribution from $e-e$, $e-p$, and $p-p$ interactions is zero when the charges are symmetric. This differs significantly from the Saha equation. By considering only the electron-proton excited bound-state contribution, it fails to capture this cancellation. When the de Broglie wavelength is similar in size to the screening length, quantum diffraction effects modify the electron distribution and the ring-sum cancellation is no longer complete. Higher order interaction terms that sample the potential at shorter distances likewise do not show a strong cancellation.

An important outcome of the expansion and reorganization of the activity series is that the low-lying bound states that appear in the calculations are unscreened. This is a consequence of regrouping terms in the basic electron-nuclei activity expansion to define new variables that optimize the convergence of the expansion at temperatures where composite particles form. The primary function of the original expansion is to obtain a global set of terms that are convergent. It is then possible to expand and regroup these terms into a more useful form.

Similar to the two-component ring sum for electrons and protons, there will be some cancellation between the $e-e$, $e-H_2^+$, and $H_2^+-H_2^+$ interactions. In the electron-proton case, the ring-diagrammatic summation, which results in the Debye-Hückel correction, includes part of the bound-state sum (Rogers 1979, 1986). The overt bound-state contribution to b_{ep} , which follows from the analytic properties of the phase shifts in equation (6), is given by

$$b_{ep}^o = 2^{1/2} \lambda_{ep}^3 Z_{PL}, \quad (12)$$

where

$$Z_{PL} = \sum_{nl} (2l + 1) \left(e^{-E_{nl}/kT} - 1 + \frac{E_{nl}}{kT} \right) \quad (13)$$

is the Planck-Larkin partition function (Larkin 1960; Rogers & Dewitt 1973; Rogers 1977; Bollé 1987, 1989; Pisano & McKellar 1989). The sum Z_{PL} is the residue after

the divergent terms in the high-temperature expansion are separated out, effectively truncating the sum at $|E_{nl}| \leq kT$. The subtractions from the Boltzmann factors in equation (13) in no way suggest that they are being discarded or cancelled by the electron-proton phase shift sum in equation (6). Instead, these divergent sums are subsumed in the diagrammatic many-body resummation. The product $z_e z_p b_{ep}^o$ is the second-order $e-p$ bound-state contribution to P/kT . At low density and temperature this factor acts linear in the activity of hydrogen atoms, while the leading plasma correction, i.e., Debye-Hückel, is 3/2 order in the activity and thus much smaller. It is in this sense that Z_{PL} represents the bound-state contribution to the EOS. Of course, the occupation numbers are still determined from Boltzmann factors and are obtained through an ancillary calculation (Rogers 1986).

From the above arguments, we expect the contribution from the highly excited electronic bound states and the scattering states of H_2 to be offset by the contribution from $e-e$ and $H_2^+-H_2^+$ scattering. The effective bound-state contribution from these states will be given by Planck-Larkin factors similar to equation (13). Their contribution to the EOS is very small and has been neglected in these calculations. Without a more complete treatment of the scattering phase shifts, the form of the contribution from lowly excited electronic states is less clear. Arguments presented in Rogers (1977, 1979) suggest that, in general, the divergent terms in the high-temperature expansion of the bound-state part of the unscreened cluster coefficients should be separated out and incorporated into the many-body calculations. In the case of H_2 , the vibrational-rotational partition function is well behaved at high temperature, while the sum over electronic bound states diverges. Based on these properties, we conjecture that the overt bound-state part of b'_{epp} will have a form similar to the following:

$$b'_{epp}{}^o = 2 \lambda_{ep}^6 \lambda_{HH}^3 e^{-E_{H_2^+}/kt} \sum_{nl} Q_{nl}(T) \left(e^{-E_{nl}/kT} - 1 + \frac{E_{nl}}{kT} \right), \quad (14)$$

where the $Q_{nl}(T)$ are the vibrational-rotational partition functions for the $H(1s)-H(n, l)$ potential energy curves. Whether this is the rigorously correct way to define the overt bound-state contribution will depend on a careful treatment of the analytic properties of the phase shifts. In a complete calculation that includes all orders of approximation, this is a mute point. In that case it is just a matter of bookkeeping. What is improperly removed one place will reappear somewhere else. Since molecules only form in substantial numbers at temperatures below 2 eV, the subtractions from the Boltzmann factors in equation (14) will have little effect on the molecular EOS. For practical calculations we can reduce equation (14) to the form

$$b'_{epp}{}^o = (b_{ep}^g)^2 b_{HH}^o, \quad (15)$$

where

$$b_{ep}^g = 2^{1/2} \lambda_{ep}^3 e^{-E_{1s}/kT}, \quad (16)$$

$$b_{HH}^o = 2^{1/2} \lambda_{HH}^3 e^{-E_{H_2}/kT} Q_{1,0}(T), \quad (17)$$

and E_{H_2} is the binding energy of H_2 molecules relative to H atoms. In the current calculations we have used the fit to

$Q_{1,0}(T)$ of the Drabowski (1984) vibrational-rotational data due to Irwin (1981, 1987, 1988). The fourth-order contribution to P/kT coming from equation (15) is $z_e^2 z_p^2 (b_{ep}^g)^2 b_{HH}^o$. Identifying $z_e z_p b_{ep}^g$ as z_H , the activity for H atoms gives the factor $z_H^2 b_{HH}^o$. This corresponds to the bound part of equation (11).

In principle the scattering-state contribution to b_{HH} should be calculated quantum mechanically as indicated in equation (11). However, the main scattering contribution comes from b_{HH}^T , which is strongly repulsive and can be calculated semiclassically from the Wigner-Kirkwood expansion. In the present calculations, as a result of the relatively high temperature, we have used only the classical limit of this expansion. The attractive and repulsive parts of the singlet potential affect the phase in different directions. When the temperature is high enough that scattering from the potential wall is the larger effect, a semiclassical calculation of the repulsive contribution should provide an estimate of the maximum size of the singlet scattering contribution. The size of the scattering contribution, $b_{HH}^{S,S}$, calculated this way is substantially smaller than b_{HH}^T , so that the sum of these two terms,

$$b_{HH}^S = b_{HH}^{S,S} + b_{HH}^T, \quad (18)$$

is a reasonable estimate of the total scattering-state contribution in equation (8). Following arguments similar to those above, we find that the H-H scattering contribution from $z_e^2 z_p^2 b_{epp}$ is given by $z_H^2 b_{HH}^S$. When the temperature is low enough that there is no appreciable ionization, the pressure to second order in the hydrogen activity reduces to the form

$$\frac{P}{kT} = z_H + z_H^2 (b_{HH}^o + b_{HH}^S). \quad (19)$$

The activity is eliminated in the usual manner through the relation

$$\rho_H = z_H \frac{\partial}{\partial z_H} \frac{P}{kT}. \quad (20)$$

In this example for pure hydrogen we have started from an activity expansion for an electron-nucleus system and arrived at equations (19) and (20). The virtue of the reorganization we have described is that it will select out the most important contributions to the EOS at arbitrary temperature and density.

In general, the issues discussed above will be the same for any molecule that has a positive molecular ion. Molecular ions, such as H_2^+ , generally have strong bonding orbitals in only the ground-state configuration and thus have convergent electronic partition functions. For these ions, the analysis leading to equation (15) is unnecessary, and the calculations are the same as for ordinary short-range interactions. This is because the reaction $p + H \leftrightarrow H_2^+$ has no effect on the total ionic charge.

2.6. Effect of Vibronic Excitations

In typical applications the temperature is low enough that only the lowest vibronic states are occupied. The current calculations span a wide range of temperature, so that at high enough temperatures the full spectrum of vibronic states can be excited. The $\langle R \rangle$ of molecular states increases as the vibronic frequency, ν , of the state increases. Conse-

quently, the interaction potential between molecules in excited vibronic states is weaker than when they are in their ground states. We have used calculations by T. N. Rescigno (2000, unpublished) to account for the effect of vibronic excitation on the H_2-H_2 and $p-H_2$ interaction potentials. These are the dominant molecular interactions in stars. Similar calculations are not available for other molecules.

When ionsphere radius is comparable to the molecular size, density effects on the core must be considered. Fortunately, the updated OPAL EOS tables do not get into this region for molecules. How density effects are handled for atomic and ionic states is described in Rogers (2001a and references therein).

3. RESULTS

The composition of stellar material is generally described in terms of just three variables, X , the hydrogen mass fraction, Y , the helium mass fraction, and Z , the mass fraction of all elements heavier than helium, known as the metallicity, so that $X + Y + Z = 1$. Following RSI96, we have tabulated data for $X = 0, 0.2, 0.4, 0.6,$ and 0.8 and for $Z = 0.00, 0.02,$ and 0.04 . Data for $X = 1.0$ have also been tabulated, so that the database for H-He mixtures spans the range from pure hydrogen to pure helium. The total contribution to the EOS from heavy elements (herein all elements heavier than helium) is at most a few percent and largely dominated by period II elements. In order to calculate accurate numerical derivatives of the EOS, a very fine grid of temperature-density data is required. Since OPAL solves directly a coupled set of activity equations for all the elements in the mixture, the inclusion of elements heavier than Ne greatly increases the computer requirements. Accordingly, RSI96 truncated the number of elements in the Grevesse et al. (1991) solar abundances by adding the abundance of elements heavier than Ne to Ne. The fractional abundances for the resulting six-element mixture are given in Table 1 of RSI96. The grid density of the EOS tables is sufficient to give interpolated values in $X, Y, Z, \rho,$ and T that are generally accurate to 0.01%, but larger errors can occur in the pressure ionization regime. Calculations of the solar EOS for a fixed metallicity with a six-element mixture reduced from Grevesse & Sauval (1998) do not affect the results to the number of significant digits of the tables.

The temperature-density ranges of the old and new EOS tables are shown in Figure 2. Also shown in Figure 2 are tracks for stars with masses of 0, 0.3, and $1 M_\odot$. The two lower mass tracks were largely outside the temperature-density range of the RSI96 tables but are completely within the range of the new tables. We have tabulated $P, E, S,$ and the following thermodynamic derivatives:

$$\chi_T = \left(\frac{\partial \ln P}{\partial \ln T} \right)_\rho, \quad \chi_\rho = \left(\frac{\partial \ln P}{\partial \ln \rho} \right)_T, \quad (21)$$

$$\Gamma_1 = \left(\frac{\partial \ln P}{\partial \ln \rho} \right)_S, \quad \frac{\Gamma_2}{\Gamma_2 - 1} = \left(\frac{\partial \ln P}{\partial \ln T} \right)_S, \quad (22)$$

$$\Gamma_3 - 1 = \left(\frac{\partial \ln T}{\partial \ln \rho} \right)_S, \quad C_V = \left(\frac{\partial E}{\partial T} \right)_V. \quad (23)$$

RSI96 also tabulated $(\partial E / \partial \rho)_T$. We have not included this derivative since it can be obtained from the thermodynamic

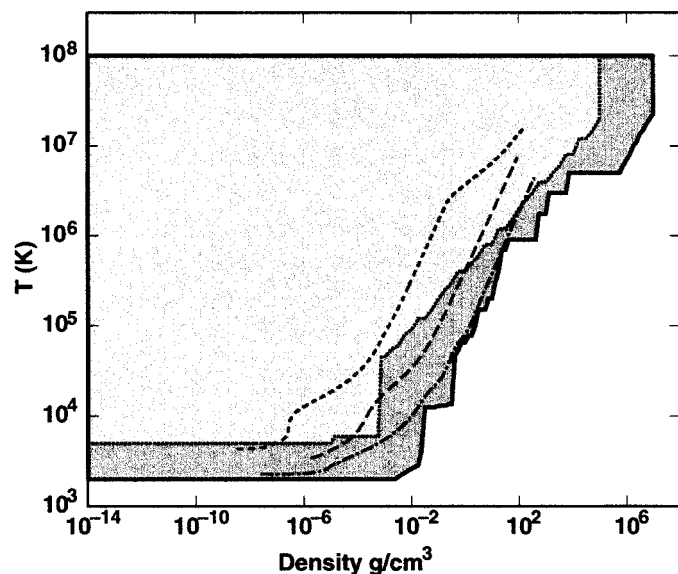


FIG. 2.—Temperature-density range of the EOS tables: range of old tables (*light-shaded region*); range of new tables (*heavy-shaded region*); $M = 1.0 M_{\odot}$ track (*short-dashed line*); $M = 0.3 M_{\odot}$ track (*long-dashed line*); $M = 0.1 M_{\odot}$ track (*dot-dashed line*).

relation $(\partial E/\partial \rho)_T = (\mu_m P/\rho^2)(1 - \chi_T)$, where μ_m is the mean molecular weight.

Some representative results from the EOS tables are shown in Figures 3–5. Figure 3 shows $\log E$ versus $\log T$ for various values of X , along an isochore having density 0.0237 g cm^{-3} . The curvature at low T is the signature for the formation of atoms and molecules. Figure 4 shows the dependence of Γ_1 on temperature for various values of X along an isochore with density 0.0056 g cm^{-3} . The dip in Γ_1 around $\log T = 5.0$ results from the formation of He^+ , the dip around $\log T = 4.5$ is due to the formation of neutral He, and the dip around $\log T = 3.7$ is due to the formation of

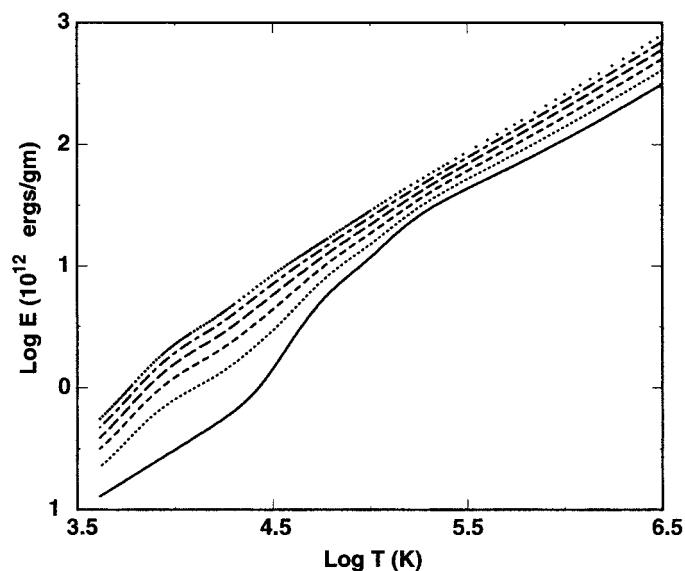


FIG. 3.—Energy vs. temperature for several values of X , zero metallicity, and density $= 0.0237 \text{ g cm}^{-3}$: $X = 0$ (*solid line*); $X = 0.2$ (*dotted line*); $X = 0.4$ (*short-dashed line*); $X = 0.6$ (*long-dashed line*); $X = 0.8$ (*dot-dashed line*); $X = 1.0$ (*squares*).

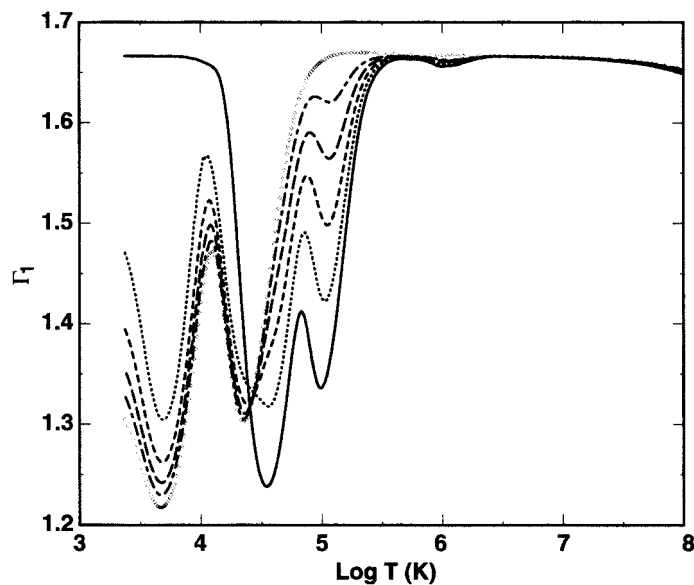


FIG. 4.— Γ_1 vs. temperature at several values of X , zero metallicity, and density $= 0.056 \text{ g cm}^{-3}$: $X = 0$ (*solid line*); $X = 0.2$ (*dotted line*); $X = 0.4$ (*short-dashed line*); $X = 0.6$ (*long-dashed line*); $X = 0.8$ (*dot-dashed line*); $X = 1.0$ (*open diamonds*).

hydrogen. The small dip in Γ_1 around $\log T = 6$ is due to the formation of heavy ions and atoms. This will be discussed further in § 4. Molecules are beginning to form at the lowest values of T , causing the slight softening of the curvature. Figure 5 shows C_v/Nk versus ρ along several isotherms with $X = 0.6$ and $Z = 0.02$. Here again the oscillatory behavior can be related to changing ionization balance as a function of density. The $Z = 0$ and $Z = 0.04$ specific heat curves (not shown) look very similar to the $Z = 0.02$ curves.

Recent stellar model calculations for low-mass stars have generally used the MDH88 or the Saumon–Chabrier–Van Horn EOS (Saumon & Chabrier 1991, 1992; Saumon,

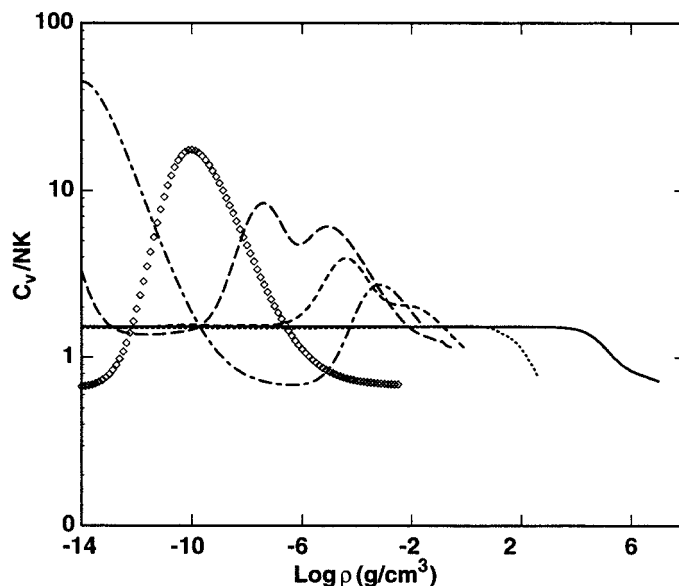


FIG. 5.—Specific heat at constant volume vs. density along several isotherms: $T = 10^8$ (*solid line*); $T = 1.35 \times 10^6$ (*dotted line*); $T = 7.75 \times 10^4$ (*short-dashed line*); $T = 1.95 \times 10^4$ (*long-dashed line*); $T = 5.88 \times 10^3$ (*dot-dashed line*); $T = 2.12 \times 10^{-3}$ (*diamonds*).

Chabrierr, & Van Horn 1995, hereafter SCVH95). The SCVH95 calculations are based on an occupation probability approach similar to MDH88. To account for interactions between atoms and the molecules, SCVH95 use realistic interaction potentials adjusted to reproduce experimental shock data, whereas MDH88 use a parameterized hard sphere model. To account for strong Coulomb coupling, SCVH95 use a screened one-component plasma model. MDH88 use the Debye-Hückel approximation to treat the Coulomb correction. This term becomes much too large when $\Gamma > 0.5$. To correct for this, they introduce a hard sphere cutoff to limit the distance of closest approach. The MDH88 and SCVH95 calculations are both being updated. One of the main improvements is in the way the occupation probability factors, w , are calculated in the Stark microfield (Potekhin, Chabrier, & Gilles 2002). SCVH95 consider only H-He mixtures, and thus their calculations are not suited to the study of seismic data.

The ratio of the OPAL pressure to the SCVH95 pressure versus temperature for 0.3 and 0.1 M_{\odot} stars is shown in Figure 6. The solar model used to calculate the temperature is described in Chabrier & Baraffe (1997). The differences for $M = 0.3 M_{\odot}$ are less than 6%, while the differences for $M = 0.1 M_{\odot}$ are as large as 20%. The increasing discrepancy with decreased stellar mass is due mainly to differences in the treatment of pressure ionization and Coulomb interactions. Both of these effects increase as M decreases. Figure 7 compares the OPAL and SCVH95 Γ_1 for a 0.1 M_{\odot} star having $X = 0.725$ and $Y = 0.275$. The noise around $\log T = 4.7$ is apparently due to the stellar model calculation used by SCVH95, since OPAL calculations for the 0.1 M_{\odot} attack from VandenBerg et al. (2000) are smooth. The OPAL EOS and opacity data are available on the World Wide Web.³

³ See <http://www-phys.llnl.gov/Research/OPAL/index.html>.

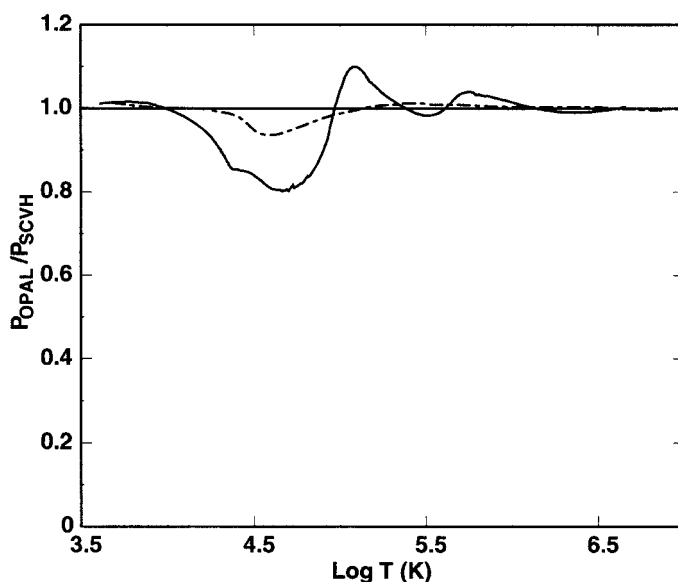


FIG. 6.—Ratio of OPAL to SCVH95 pressure vs. temperature along solar tracks calculated by Chabrier (Chabrier & Baraffe 1997): $M = 0.3 M_{\odot}$ (dot-dashed line); $M = 0.1 M_{\odot}$ (solid line).

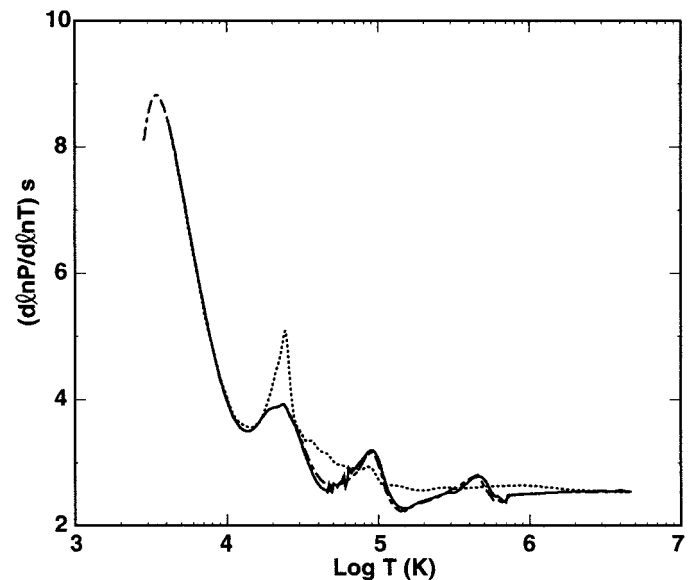


FIG. 7.—Comparison of OPAL and SCVH95 Γ_1 vs. $\log T$ for $M = 0.1 M_{\odot}$: SCVH95 for Chabrier solar track (dotted line); OPAL for Chabrier track (solid line); OPAL for VandenBerg track (dot-dashed line).

4. HELIOSEISMOLOGY

Experimental measurements of the thermodynamic properties of materials heated to stellar interior conditions are very limited. The extant measurements utilize various methods for generating intense shock waves in a sample material. The EOS is then obtained through the Rankine-Hugoniot relations. The shock measurements are mainly limited to the low-temperature end of tracks of low-mass stars and giant planets. The error bars can be substantial. Fortunately, in the special case of the Sun, the seismic data provide very detailed information on the solar interior and indirectly the EOS. The determination of internal structure relies on a very accurate measurement of the solar oscillation frequencies and a solar model whose theoretical frequencies are very close to those of the Sun. In this approach detailed measurements of the oscillation frequencies are inverted to calculate the difference, $\delta\Gamma_1(r/R)$, between the Sun and a standard reference model. The smaller the magnitude of $\delta\Gamma_1(r/R)$, the greater the confidence in the solar model. Because of the high accuracy of the observational data, the functional form of $\delta\Gamma_1(r/R)$ can suggest where the model needs to be improved. The calculation of solar structure depends on a number of things, such as models for convection and particle diffusion, nuclear reaction rates, opacity, and EOS. In principle, there are magnetic field perturbations of the oscillation frequencies and turbulence effects near the bottom of the convection zone, but in most studies they are neglected.

EK98 have given an excellent example of seismic data being able to detect shortcomings in the EOS theory. They were concerned with why the inferred $\delta\Gamma_1$ obtained from inversions based on model S of Christensen-Dalsgaard et al. (1996) diverge away from zero as $r/R \rightarrow 0$ (Dziembowski, Pamyatnykh, & Sienkiewicz 1992; Antia & Basu 1994). They were able to demonstrate that this divergence was due to a small relativistic effect not included in the EOS calculations. Since $kT/m_e c^2$ is only 0.029 at the solar center, this correction was not included in the MDH88 and OPAL EOS

calculations. These effects have recently been included in the free electron contribution to the MDH88 calculations (Gong, Däppen, & Zejda 2001b). In general, the reason for the discrepancy between theory and observation is not so clear. Significant discrepancies (compared to the accuracy of the seismic data) between the Sun and the theoretical models are also present in the near-surface regions ($r/R > 0.97$) and near the base of the convection zone, the sources of which are still being investigated.

The total $\delta\Gamma_1(r)$ between the Sun and the present calculations is composed of a direct part resulting from the change in the EOS and an implicit part resulting from a modification of the theoretical oscillation frequencies of the solar model. In the following, since only the EOS has changed, we follow EK98 and consider only the direct contribution so that

$$\delta\Gamma_1 = \delta\Gamma_1^{\text{old}} + (\Gamma_1^{\text{new}} - \Gamma_1^{\text{old}}) = \Gamma_1^{\text{new}} - \Gamma_1^{\text{Sun}}, \quad (24)$$

where $\delta\Gamma_1^{\text{old}}$ is the inferred $\delta\Gamma_1$ from EK98 based on the RSI96 EOS.

Figure 8 compares the new $\delta\Gamma_1(r/R)$ with the nonrelativistic $\delta\Gamma_1(r/R)$ used in the EK98 calculations. The flattening of $\delta\Gamma_1$ compared to RSI96 for $r/R < 0.5$ is due to relativistic effects (see Fig. 2 of EK98). The error bars imposed on the new result indicate the estimated size of the errors resulting from inversion of the seismic data. The somewhat larger discrepancy for $r/R > 0.97$ present in the earlier calculations is little changed in the new calculations.

Gong, Däppen, & Nayfonov (2001a) carried out an extensive investigation of the effect of heavy elements on Γ_1 . They found that elements heavier than Ne affect the value of Γ_1 by at most 3×10^{-4} . In the present work we found the still small but slightly larger value of 5×10^{-4} at temperatures around 2×10^6 . Differences elsewhere were typically at most 1×10^{-4} (see Fig. 13). At the current level of discrepancy between the Sun and EOS models, the reduction to six elements is adequate. Gong et al. (2001a) also give extensive comparisons between MDH88 and OPAL.

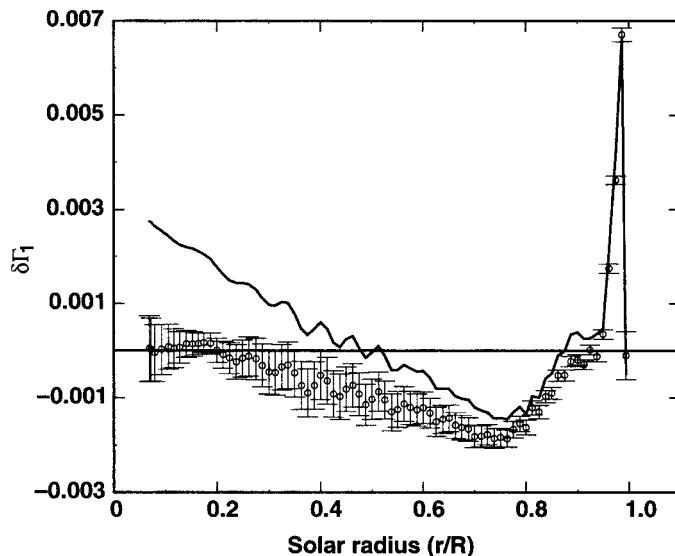


Fig. 8.—Sun-OPAL $\delta\Gamma_1$ vs. r/R : RSI96 (solid line); updated OPAL (open circles). Error bars are taken from the EK98 inversion of seismic data.

In the near-surface region the MDH88 $\delta\Gamma_1$ discrepancy with the Sun is somewhat smaller than OPAL (see Fig. 3 of EK98). It has been suggested that a large part of the discrepancy may lie in the different treatments of excited states between MDH88 and OPAL (Nayfonov & Däppen 1998; Basu, Däppen, & Nayfonov 1999; Gong et al. 2001a). Looking for other possibilities, we note that the shapes of the discrepancy between MDH and OPAL with the Sun are qualitatively similar, indicating that the primary source of the discrepancy may be the same in both cases. This could indicate some shortcoming in the EOS theory, but it could also point to shortcomings in the stellar structure calculations. Approximations in the modeling of convection, turbulence, diffusion, etc., in the solar model could produce a $T(r/R)$ and $\rho(r/R)$ that are slightly different than the intrinsic solar values.

We expect Γ_1 to be most sensitive to changes in temperature. Consequently, some theoretical inaccuracy in $T(r/R)$ could affect the calculated value of $\Gamma_1(r/R)$. Figure 9 shows the sensitivity of $\delta\Gamma_1$ to reductions in temperature along the model S track of 1% and 3%. This change has a substantial effect in the middle of the He ionization around $r/R = 0.98$ but only a small effect elsewhere. Clearly any physics modification that could affect $T(r/R)$ by a few percent in the 40,000–70,000 K region would produce discrepancies of the size reported.

In recent years the estimated value of Y in the convection zone has fluctuated between about 0.23 and 0.26, with a current estimate of 0.245 obtained from inversions using model S. Figure 10 shows the sensitivity of $\delta\Gamma_1$ to changes in Y . A 4% increase in Y to 0.255 would considerably reduce the discrepancy with the Sun in the $0.94 \leq r/R \leq 0.975$ region, whereas an 8% increase to 0.265 is tending toward increased discrepancies. A combination of physics improvements that affect the temperature and a modification of Y could also explain the discrepancies. We present these sensitivity examples as a basis for further investigation.

The metallicity of the Sun as a function of depth is also uncertain. Its value at the solar surface can be determined from spectrographic observations. It is often assumed that

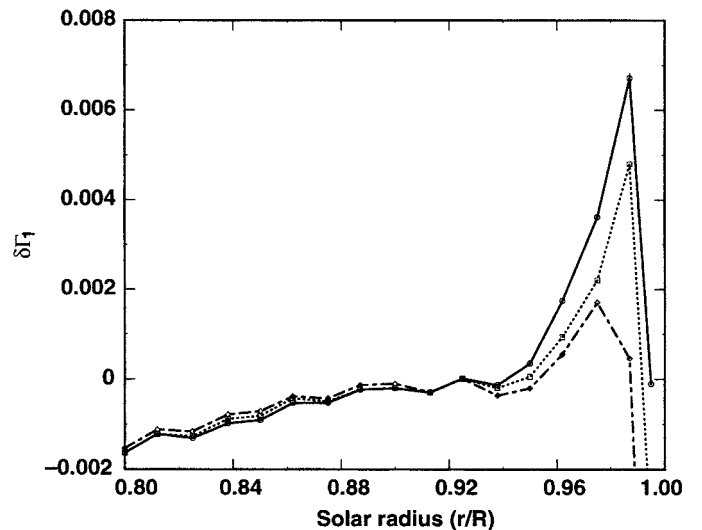


Fig. 9.—Sensitivity of $\delta\Gamma_1$ to changes in temperature. Model S solar track temperatures (solid line); model S temperatures reduced by 1% (dotted line) and 3% (dot-dashed line).

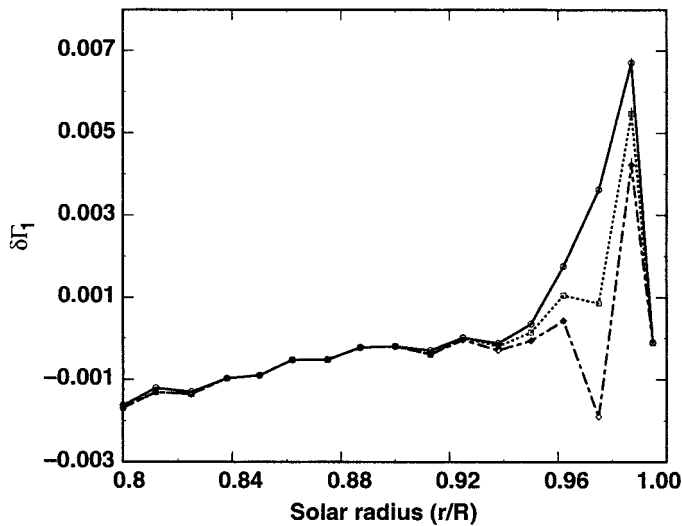


FIG. 10.—Sensitivity of $\delta\Gamma_1$ to increases in helium abundance along the model S track. Y is varied at the expense of X for fixed Z : no enhancement (solid line); 4% enhancement in value of Y (dotted line); 8% enhancement (dot-dashed line).

the heavy-element mass content and the relative abundance of the elements that comprise Z are the same at all depths. Nevertheless, gravitational settling and radiative diffusion can lead to variations in both Z and its composition as a function of depth. Recent calculations (Bahcall & Pinsonneault 1995; Turcotte & Christensen-Dalsgaard 1998; Turcotte et al. 1998) find this to be a relatively small effect for CNO, the primary heavy-element contributors to Γ_1 . Abundance changes as a result of these processes are typically less than 10%.

We note that helioseismic observations may be able to predict Z and its variation with depth. This is suggested by Figure 11, which shows Γ_1 versus T along a solar track for three metallicities: zero, solar, and twice solar, keeping X fixed at its value along the model S track. The zero-metallic-

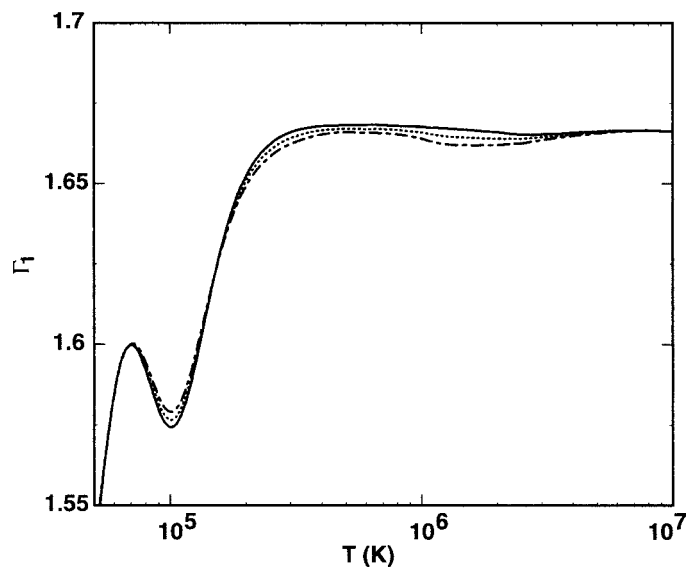


FIG. 11.—Solar Γ_1 vs. T with X fixed at model S value. Z is varied at the expense of Y : zero metallicity (solid line); solar metallicity (dotted line); twice-solar metallicity (dot-dashed line).

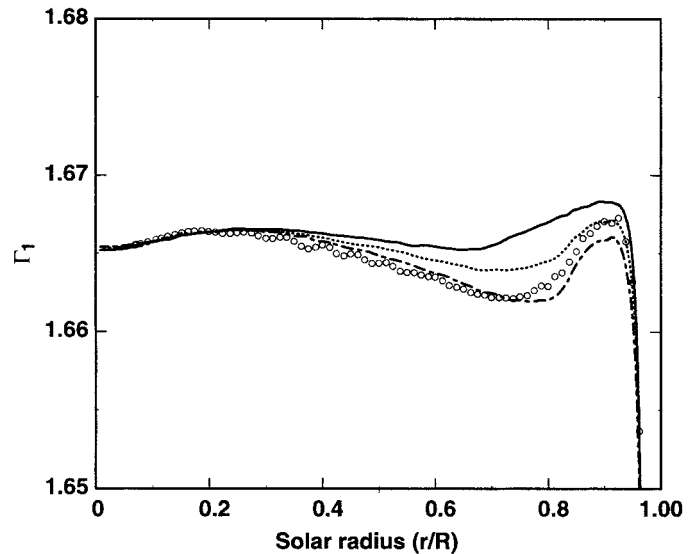


FIG. 12.—Solar Γ_1 vs. r/R for several metallicities compared to the inferred Γ_1 obtained from eq. (24) with the new opal EOS: zero metallicity (solid line); solar metallicity (dotted line); twice-solar metallicity (dot-dashed line); inferred Γ_1 (open circles). Approximated error bars related to the inversion are represented by the size of the circles.

ity Γ_1 shows a slight minimum around $T = 2 \times 10^6$ K, corresponding to the region where the radiation correction gives the largest reduction in Γ_1 . The solar and twice-solar metallicity curves display an increasing minimum around $T = 1.5 \times 10^6$ K, as a result of multiple ionization of heavy elements. There is a second depression around $T = 10^5$ K related to helium ionization. In this case the depression decreases with increasing Z . This is due to the reduced amount of He available to create the depression as metallicity increases at the expense of He. The shape of Γ_1 as a function of depth thus displays a clear signature of the metallicity. Because of the low metallicity in the Sun, this is a small effect. Nevertheless, because of the high accuracy of the observational data, it can be tested.

Figure 12 compares the inferred Γ_1 obtained from the current EOS calculations (eq. [24]) with the zero, solar, and twice-solar metallicity curves in the range of the high-temperature depression. The agreement with the solar metallicity curve is quite good down to r/R around 0.85. With increasing depth, this is followed by a transition to the twice-solar metallicity curves as the bottom of the convection zone is approached. For greater depths the inferred Γ_1 is quite close to the twice-solar metallicity curve. The implications of this are unclear. It may simply be that the neglected corrections to equation (24) are significant. Turck-Chieze (1998) has presented evidence that the abundance of CNO may need to be increased by about 15%. Increasing the CNO abundances could provide a partial answer to the discrepancy. On the other hand, Fukugita & Hata (1998) find that metallicity increases greater than 40% in the solar core ($r/R < 0.25$) are incompatible with solar neutrino experiments. It is interesting to note that the conditions around $r/R = 0.71$ are of no special significance to the EOS, whereas it is a very special location in the Sun, separating the radiation zone from the convection zone. Whether this is merely a coincidence or points to some shortcoming in the solar model and/or calculation of $\delta\Gamma_1$ awaits further investigation.

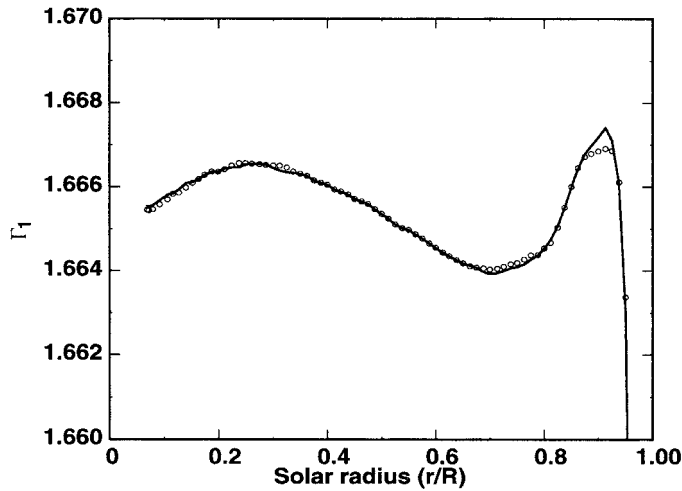


FIG. 13.—Sensitivity of Γ_1 to number of elements included in the mixture: six-element mixture truncated from Grevesse et al. (1991) solar abundances (solid line); 14-element mixture truncated from same abundance data (open circles).

There is remarkable agreement between the inferred Γ_1 and the three metallicity curves for $r/R < 0.35$. In the inner region the heavy elements are nearly completely ionized and thus Γ_1 is not sensitive to metallicity. In the ideal case that the observations, the input physics, and the solar model are all accurately known, leaving the metallicity as the only free parameter, it should be possible, for the region above $r/R > 0.35$, to estimate the metallicity as a function of depth by an iterative procedure.

In the present work we have calculated EOS tables based on a six-element mixture truncated from the Grevesse et al. (1991) solar abundances. In order to test whether interpolation in the data tables or the truncation of the Grevesse et al. (1991) abundances to a six-element mixture significantly affects the comparison in Figure 11, we have done calculations with input taken directly from the model S data set, both for the six-element mixture and a 14-element mixture reduced from the same abundances (see Table 1 of Iglesias, Rogers, & Wilson 1992). Figure 13 compares the differences in $\delta\Gamma_1$ (eq. [24]) between the truncated six-element mixture and the 14-element mixture. The differences are quite small except in the vicinity of $r/R = 0.92$, where the temperature is around 10^6 K. This is due to the multiple ionization of heavy elements. Some small differences (not shown in the figure) also occur near the surface. The interpolated six-element $\delta\Gamma_1$ agrees with direct evaluation to within 0.01%.

5. DISCUSSION

We have reported herein on updated and expanded OPAL EOS tables. These tables replace the 1996 version of RSI96. The RSI96 tables only cover a temperature-density range suitable for modeling stars more massive than about $0.8 M_\odot$, whereas the new tables are suitable for stars more massive than about $0.1 M_\odot$. The differences compared to

RSI96 are small except at high temperature and density where relativistic effects not included in RSI96 make a difference. The new tables go down to 2000 K, whereas the RSI96 tables did not go below 5000 K. As a result, atoms and molecules play a more important role. At temperature-density conditions where neutrals and ions exist simultaneously, this causes convergence problems for the activity expansion. These convergence problems were handled by developing a hybrid expansion that combines the best features of the activity and virial expansions. Another problem that arises in connection with molecules is how to handle the long-range interactions between molecular ions and other ionic species and the divergence of certain molecular partition functions. We were not able to give rigorous solutions to these issues. However, we were able to draw on analogies with the atomic case to arrive at reasonable approximations.

Because of the low metallicity of main-sequence stars, the correction to the H-He EOS is only a few percent, due mostly to period II elements. Nevertheless, there are applications where differences of this size are significant; this is especially true in the analysis of seismic data. In most other EOS calculations individual element tables are calculated and mixed using ideal gas relations. OPAL numerically solves a fully coupled set of activity equations. This distinction can be important in opacity calculations since a careful treatment of the coupling between unlike species can affect the occupation numbers. For the EOS calculations reported herein we have again assumed a six-element mixture composed of H, He, C, N, O, and Ne.

Helioseismology is a very important tool for constraining theories of the solar interior (Bahcall et al. 1997; Basu, Pinsonneault, & Bahcall, 2000; Bahcall, Pinsonneault, & Basu 2001) and has been used to rule out a number of mechanisms proposed to explain the missing neutrinos. When discrepancies arise between seismic observations and theoretical models, it is very important to try to isolate the source of the discrepancy, since it could point to some shortcoming in the solar model. There have been small but persistent differences between the inferred solar Γ_1 and EOS theories. In order to stimulate studies to determine the source of these discrepancies, we have presented some sensitivity calculations. We have also suggested that a small effect on the shape Γ_1 , due to the multiple ionization of heavy elements in the vicinity of the bottom of the convection zone, can be used to determine the metallicity in this region.

We are grateful to Werner Däppen and Hugh Dewitt for numerous helpful discussions. Alexander Kosovichev provided the model S data and helpful comments on the analysis of helioseismic data. Gilles Chabrier provided the SCVH95 EOS data for 0.1 and $0.3 M_\odot$ tracks. Don Vandenberg graciously calculated some solar tracks for low-mass stars. This work was performed under the auspices of the US Department of Energy by Lawrence Livermore National Laboratory under contract W-7405-Eng-48 and was supported in part by grant AST-99-87391 of the National Science Foundation.

REFERENCES

- Antia, H. M., & Basu, S. 1994, *ApJ*, 426, 801
 Aparico, J. M. 1998, *ApJS*, 117, 627
 Bahcall, J. N., & Pinsonneault, M. H. 1995, *Rev. Mod. Phys.*, 67, 781
 Bahcall, J. N., Pinsonneault, M. H., & Basu, S. 2001, *ApJ*, 555, 990
 Bahcall, J. N., Pinsonneault, M. H., Basu, S., & Christensen-Dalsgaard, J. 1997, *Phys. Rev. Lett.*, 78, 171
 Basu, S., Däppen, W., & Nayfonov, A. 1999, *ApJ*, 518, 985
 Basu, S., Pinsonneault, M. H., & Bahcall, J. N. 2000, *ApJ*, 529, 1084

- Beth, E., & Uhlenbeck, G. E. 1937, *Physica*, 3, 915
- Bollé, D. 1987, *Phys. Rev. A*, 36, 3259
- . 1989, *Phys. Rev. A*, 39, 2752
- Chabrier, G., & Baraffe, I. 1997, *A&A*, 327, 1039
- Christensen-Dalsgaard, J., et al. 1996, *Science*, 272, 1286
- Cox, J., & Guili, R. 1968, *Principles of Stellar Evolution* (New York: Gordon and Beach)
- Cvetko, D., et al. 1994, *J. Chem. Phys.*, 100, 2052
- Däppen, W., Anderson, L. S., & Mihalas, D. 1987, *ApJ*, 319, 195
- Diep, P., & Johnson, K. J. 2000, *J. Chem. Phys.*, 112, 4465
- Drabowski, I. 1984, *Canadian J. Phys.*, 62, 1639
- Dziembowski, W. A., Pamyatnykh, A. A., & Sienkiewicz, R. 1992, *Acta Astron.*, 14, 5
- Elliot, J. R., & Kosovichev, A. G. 1998, *ApJ*, 500, L199 (EK98)
- Fukugita, M., & Hata, N. 1998, *ApJ*, 499, 513
- Gong, Z., Däppen, W., & Nayfonov, A. 2001a, *ApJ*, 563, 419
- Gong, Z., Däppen, W., & Zejda, L. 2001b, *ApJ*, 546, 1178
- Gong, Z., Zejda, L., Däppen, W., & Aparico, J. M. 2001c, *Comput. Phys. Commun.*, 136, 294
- Grevesse, N., Lambert, D. L., Sauval, A. J., van Dishoeck, E. F., Farmer, C. B., & Naton, R. H. 1991, *A&A*, 242, 488
- Grevesse, N., & Sauval, A. J. 1998, *Space Sci. Rev.*, 85, 161
- Hopper, D. G. 1980, *J. Chem. Phys.*, 73, 9
- Hummer, D. G., & Mihalas, D. 1988, *ApJ*, 331, 794
- Iglesias, C. A., & Rogers, F. J. 1996, *ApJ*, 464, 943
- Iglesias, C. A., Rogers, F. J., & Wilson, B. G. 1992, *ApJ*, 397, 717
- Irwin, A. W. 1981, *ApJS*, 45, 621
- . 1987, *A&A*, 182, 348
- . 1988, *A&AS*, 74, 145
- Kolos, W., & Peek, J. M. 1976, *J. Chem. Phys.*, 12, 381
- Kolos, W., & Wolniewicz, L. 1965, *J. Chem. Phys.*, 43, 2429
- Larkin, A. I. 1960, *Soviet Phys.-JETP Lett.*, 11, 1363
- Mihalas, D., Däppen, W., & Hummer, D. G. 1988, *ApJ*, 331, 815 (MDH88)
- Nayfonov, A., & Däppen, W. 1998, *ApJ*, 499, 489
- Partridge, H., Bauschlicher, C. W., Stallcop, J. R., & Levin, E. 1993, *J. Chem. Phys.*, 99, 5951
- Pisano, C., & McKeller, M. J. 1989, *Phys. Rev. A*, 40, 6597
- Potekhin, A. Y., Chabrier, G., & Gilles, D. 2002, *Phys. Rev. E*, 65, 036412
- Rogers, F. J. 1974, *Phys. Rev. A*, 10, 2441
- . 1977, *Phys. Lett.*, 61A, 358
- . 1979, *Phys. Rev. A*, 19, 375
- . 1981, *Phys. Rev. A*, 24, 1531
- . 1986, *ApJ*, 310, 723
- . 1988, *Phys. Rev. A*, 38, 5001
- . 1994, in *Equation of State in Astrophysics*, ed. G. Chabrier & E. Schatzmann (Cambridge: Cambridge Univ. Press), 16
- . 2001a, *Contrib. Plasma Phys.*, 41, 179
- . 2001b, *Phys. Plasmas*, 7, 51
- Rogers, F. J., & Dewitt, H. E. 1973, *Phys. Rev. A*, 8, 1061
- Rogers, F. J., Swenson, F. J., & Iglesias, C. A. 1996, *ApJ*, 456, 902 (RS196)
- Saumon, D., & Chabrier, G. 1991, *Phys. Rev. A*, 44, 5122
- . 1992, *Phys. Rev. A*, 46, 2084
- Saumon, D., Chabrier, G., & van Horn, H. M. 1995, *ApJS*, 99, 713 (SCvH95)
- Schlages, M., & Kremp, D. 1982, *Ann. Phys.*, 7, 69
- Shafer, R., & Gordon, R. G. 1973, *J. Chem. Phys.*, 57, 5422
- Sharp, T. E. 1971, *At. Data*, 2, 119
- Stoltzmann, W., & Blöcker, T. 1996, *A&A*, 314, 1024
- Sugar, R. P. 1991, *Comput. Phys. Commun.*, 66, 233
- Tank, K. T., & Yang, X. D. 1990, *Phys. Rev. A*, 42, 311
- Teller, E. 1930, *Z. Phys.*, 61, 458
- Turck-Chièze, S. 1998, *Space Sci. Rev.*, 85, 125
- Turcotte, S., & Christensen-Dalsgaard, J. 1998, *Space Sci. Rev.*, 85, 133
- Turcotte, S., Richer, J., Michaud, G., Iglesias, C. A., & Rogers, F. J. 1998, *ApJ*, 504, 539
- VandenBerg, D. A., Swenson, F. J., Rogers, F. J., Iglesias, C. A., & Alexander, D. R. 2000, *ApJ*, 532, 430
- Waech, T. G., & Bernstein, R. B. J. 1967, *Chem. Phys.*, 46, 4905